

Logarithmic singularities and quantum oscillations in magnetically doped topological insulators

D. Nandi,¹ Inti Sodemann,^{2,3} K. Shain,¹ G.H. Lee,^{1,4} K.-F. Huang,¹ Cui-Zu Chang,^{5,6} Yunbo Ou,⁵ S.P. Lee,^{7,8} J. Ward,¹ J.S. Moodera,⁵ P. Kim,¹ and A. Yacoby¹

¹*Department of Physics, Harvard University, Cambridge, MA 02138, USA*

²*Max-Planck Institute for the Physics of Complex Systems, D-01187 Dresden, Germany*

³*Department of Physics, Massachusetts Institute of Technology, Cambridge, MA 02139, USA*

⁴*Department of Physics, Pohang University of Science and Technology, Pohang 790-784, Republic of Korea*

⁵*Francis Bitter Magnet Lab, Massachusetts Institute of Technology, Cambridge, MA 02139, USA*

⁶*The Center for Nanoscale Science and Department of Physics, The Pennsylvania State University, University Park, PA 16802-6300, USA*

⁷*Department of Physics, University of Alberta, Edmonton, Alberta T6G 2E1, Canada*

⁸*Department of Physics and Astronomy, The Johns Hopkins University, Baltimore, Maryland 21218, USA*

(Dated: April 17, 2018)

We report magnetotransport measurements on magnetically doped $(\text{Bi,Sb})_2\text{Te}_3$ films grown by molecular beam epitaxy. In Hallbar devices, we observe logarithmic dependence of transport coefficients in temperature and bias voltage which can be understood to arise from electron - electron interaction corrections to the conductivity and self-heating. Submicron scale devices exhibit intriguing quantum oscillations at high magnetic fields with dependence on bias voltage. The observed quantum oscillations can be attributed to bulk and surface transport.

PACS numbers: 75.30.Hx, 73.20.At, 73.20.-r, 72.25.Dc, 85.75.-d

I. INTRODUCTION

Breaking of time reversal symmetry in topological insulators can unlock exotic phenomenon such as the quantized anomalous Hall effect¹⁻⁵, giant magneto-optical Kerr and Faraday effects⁶, the inverse spin-galvanic effect⁷, image magnetic monopole effect⁸ and chiral Majorana modes^{9,10}. Angle resolved photoemission spectroscopy measurements have revealed presence of a magnetic gap at the Dirac point as well as hedgehog spin texture in magnetic topological insulators^{11,12}. Proximity coupling to a magnetic insulator such as EuS, yttrium iron garnet, and thulium iron garnet¹³⁻¹⁵ or introducing magnetic dopants like Mn, Cr and V^{2,3,16} can remove time reversal symmetry. Such efforts have induced long range ferromagnetic order in topological insulators.

In this paper we explore magnetotransport in magnetically doped ultrathin films of $(\text{Bi,Sb})_2\text{Te}_3$ to understand the role of different scattering mechanisms. By studying the effect of temperature and voltage bias on the longitudinal and anomalous Hall resistances, we observe logarithmic dependences on temperature and voltage bias. Joule heating due to voltage bias increases the effective temperature of the hot electrons¹⁷. The logarithmic singularities are originating from interplay of electron-electron interaction and disorder. We find that our observed logarithmic corrections quantitatively agree with the Alshuler-Aranov theory of electron-electron interactions. Furthermore, in submicron sized mesoscale devices we observe quantum oscillations that depend on voltage bias and weaken with increasing sample width.

II. MATERIALS AND METHODS

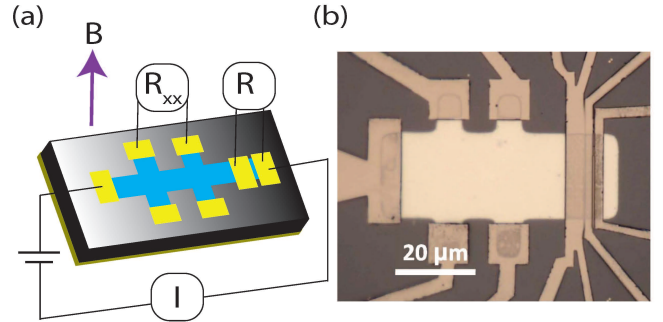


FIG. 1. (color online) (a) Schematics of a magnetic topological insulator device. (b) Optical image of a Hallbar device H_1 and a two terminal device D_1 simultaneously patterned on magnetically (Vanadium) doped topological insulators.

The 4 quintuple layers (QLs) thick pristine and V-doped $(\text{Bi,Sb})_2\text{Te}_3$ films are grown on SrTiO_3 (111) substrate by molecular beam epitaxy (MBE). The growth process was monitored in-situ by reflection high-energy electron diffraction (RHEED) to ensure high quality films^{3,18,19}. To prevent oxidation, a capping layer of 10 nm tellurium was deposited. The devices were fabricated employing standard photolithography and electron-beam lithography techniques. The device schematic and optical image of a Ti/Nb/NbN contacted magnetic topological insulator film is shown in Figs. 1(a)-1(b). The transport measurements were done in a ^3He - ^4He dilution refrigerator using standard ac lock-in measurement techniques. Here we summarize results from a pristine Hallbar device H_0 , a V-doped Hallbar device H_1 and a V-doped

submicron scale device D_1 .

III. RESULTS AND DISCUSSION

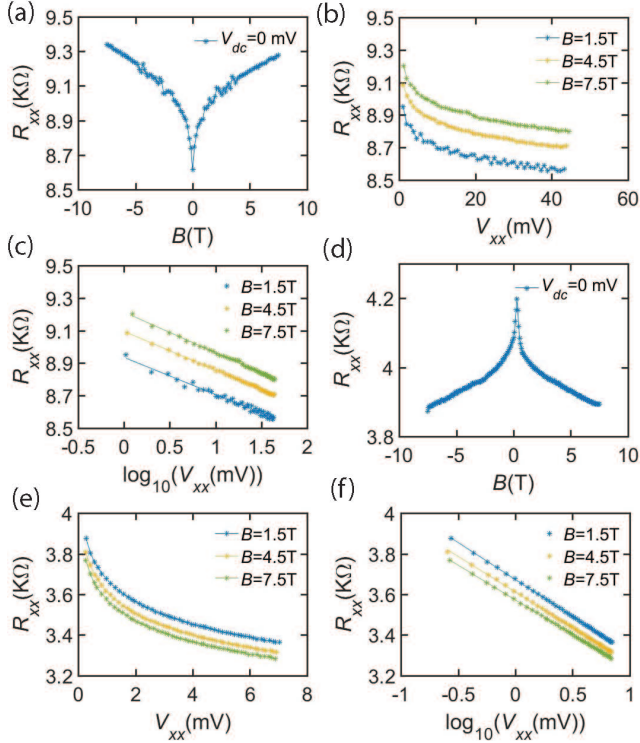


FIG. 2. Comparison of magnetotransport in pristine and V-doped 4 QL thick $(\text{Bi,Sb})_2\text{Te}_3$ films. (a) Magnetoresistance dip at $B=0$ T in the sweep range $B = -7.5$ to $+7.5$ T for pristine $(\text{Bi,Sb})_2\text{Te}_3$ samples. (b) Bias dependence of pristine $(\text{Bi,Sb})_2\text{Te}_3$ film at $B = 1.5, 4.5$ and 7.5 T. (c) Logarithmic plot for bias dependence of 4 QL pristine $(\text{Bi,Sb})_2\text{Te}_3$ film at $B = 1.5, 4.5$ and 7.5 T. (d) Magnetoresistance peak at $B=0$ T in the sweep range $B = -7.5$ to $+7.5$ T for V-doped $(\text{Bi,Sb})_2\text{Te}_3$. (e) Bias dependence of V-doped $(\text{Bi,Sb})_2\text{Te}_3$ film at $B = 1.5, 4.5$ and 7.5 T. (f) Logarithmic plot for bias dependence of V-doped $(\text{Bi,Sb})_2\text{Te}_3$ film at $B = 1.5, 4.5$ and 7.5 T.

Magnetotransport measurements in a Hallbar device H_0 on pristine 4QL $(\text{Bi,Sb})_2\text{Te}_3$ films presented in Fig. 2(a) exhibit a dip in the longitudinal resistance R_{xx} at $B = 0$ T which is attributed to weak antilocalization effect^{20,21}. This is because in the presence of strong spin-orbit coupling time reversed trajectories have opposite spin orientations which lead to a destructive interference and a resistance minimum²².

We measured the bias dependence of longitudinal resistance R_{xx} in the same device. The results are shown in Fig. 2(b) - Fig. 2(c) for a few different magnetic fields and exhibit a logarithmic dependence on voltage bias. Weak antilocalization is in itself a possible cause of logarithmic correction. However lowering temperature or voltage bias is expected to make weak antilocaliza-

tion effect more pronounced thereby decreasing resistivity which is inconsistent with Fig. 2(b) - Fig. 2(c).

Further by introducing magnetic impurities, the weak antilocalization effects can be heavily suppressed as has been reported in Fe-doped Bi_2Te_3 and Cr-doped Bi_2Se_3 films²³⁻²⁵. Fig. 2(d) shows the magnetoresistance in a V-doped $(\text{Bi,Sb})_2\text{Te}_3$ has a peak instead of a dip at $B = 0$ T seen in pristine samples. Even when the weak antilocalization effects are suppressed, the longitudinal resistance R_{xx} in V-doped $(\text{Bi,Sb})_2\text{Te}_3$ has a logarithmic dependence on voltage bias as shown in Fig. 2(e) - Fig. 2(f) at different magnetic fields.

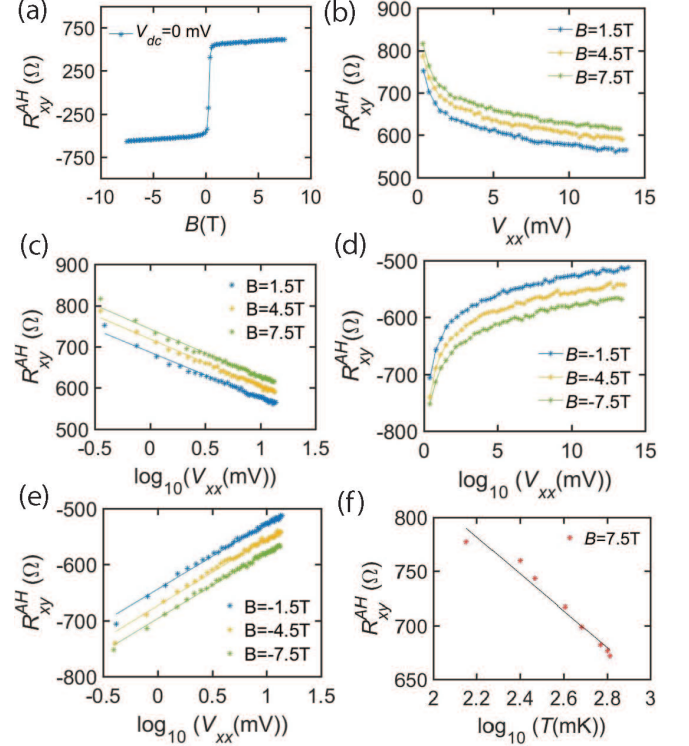


FIG. 3. (color online) Voltage bias and temperature dependence of anomalous Hall effect of V-doped 4 QL thick $(\text{Bi,Sb})_2\text{Te}_3$ films. (a) Magnetic field dependence of anomalous hall resistance R_{xy}^{AH} measured at $V_{dc} = 0$. (b) Bias dependence of R_{xy}^{AH} at $B = 1.5, 4.5$ and 7.5 T. (c) Logarithmic plot for bias dependence of R_{xy}^{AH} at $B = 1.5, 4.5$ and 7.5 T. (d) Bias dependence of R_{xy}^{AH} at $B = -1.5, -4.5$ and -7.5 T. (e) Logarithmic plot for bias dependence of R_{xy}^{AH} at $B = -1.5, -4.5$ and -7.5 T. (f) R_{xy}^{AH} exhibits a logarithmic dependence on temperature at $B = 7.5$ T in the temperature range of 140 mK to 650 mK .

Weak localization in disordered two dimensional (2D) systems is also a potential explanation for logarithmic increase in resistance at low temperatures. The existence of weak localization relies on the existence of coherent constructive interference of time reversed trajectories for an electron to return to the origin²⁶. Moderate external magnetic fields as well as magnetic impurities, that break time reversal symmetry, are typically enough to

suppress logarithmic corrections arising from weak localization²⁷⁻²⁹. However, the logarithmic corrections observed in our experiments persist even at fields of 7.5 T.

A way to identify logarithmic corrections due to weak localization is by the absence of logarithmic corrections to R_{xy} ^{27,28,30}. In Fig. 3(a) anomalous Hall measurements are shown without an applied bias. The R_{xy}^{AH} jumps at the coercive field when the magnetization switches its direction. Fig. 3(b)- Fig. 3(c) shows that the logarithmic dependence on voltage bias are present in anomalous Hall resistance R_{xy}^{AH} as well. The data is antisymmetric in magnetic field as shown in Fig. 3(d)- Fig. 3(e) because of which we can rule out spurious R_{xx} contributions. Interestingly, if instead of bias voltage temperature of the sample is changed, similar decrease in resistance R_{xy}^{AH} is observed as shown in Fig. 3(f). Therefore, weak localization cannot explain the transport behavior that we observe.

Logarithmic corrections to conductance could also arise from scattering off magnetic impurities as in the Kondo effect³¹⁻³³. However, in the ferromagnetic state magnetic spin-flips should become increasingly energetically unfavorable at low temperatures and at large external magnetic fields. More importantly, the fact that logarithmic dependences are also observed in topological insulator thin films in the absence of magnetic dopants^{34,35} makes this scenario an unlikely explanation of our findings.

Magneto-transport studies in pristine topological insulator Bi_2Se_3 films found it crucial to include electron-electron interactions^{34,35}. We explain why the observed logarithmic singularities are due to electron-electron interactions in the 2D surface states. As first realized by Altshuler and Aronov³⁶ (AA) disordered 2D electron systems exhibit a breakdown of the Fermi-Liquid theory due to reduced ability of the disordered electron gas to screen the Coulomb interaction. The logarithmic corrections in the AA theory are pervasive and are expected to arise not only in transport properties but also in equilibrium thermodynamic quantities such as specific heat²⁸. One of the key differences of the AA corrections with those in the localization theory is that both the longitudinal and Hall resistivities are expected to acquire logarithmic corrections^{27,28}. In fact the logarithmic corrections are most easily expressed in terms of conductivities rather than resistivities in the AA theory, because the Hall conductivity is expected to remain unchanged. Specifically one expects the logarithmic corrections in the AA model to be given by²⁷⁻²⁹:

$$\delta\sigma_{xx}(\varepsilon) = \kappa \frac{e^2}{h} \log\left(\frac{\varepsilon\tau}{\hbar}\right), \quad \delta\sigma_{xy} = 0, \quad (1)$$

where τ is the elastic scattering time, and ε is an appropriate energy scale that can be chosen to be the largest among the temperature $k_B T$ or the frequency $\hbar\omega$, at which the conductivity is probed. κ is a dimensionless number that takes different values for spinless and spinful electrons, and depends on a dimensionless parameter

F that characterizes a Hartree contribution to the conductivity corrections^{28,29,37}. This parameter takes the following forms for spinless and spinful electrons:

$$\kappa^{\text{spinless}} = \frac{1}{2\pi}, \quad (2)$$

$$\kappa^{\text{spinfull}} = \frac{1}{2\pi}(2 - 2F), \quad (3)$$

For short range interaction, $F=1$ and long range interaction $F=0$ ³⁸. For spin-split bands one expects that for a spin splitting $\Delta \gg k_B T$, the only singular logarithmic terms arise from exchange and $S_z = 0$ Hartree contributions, and the expression for κ is²⁸:

$$\kappa^{\text{spin-split}} = \frac{1}{2\pi}(2 - F) \approx 0.32 \left(1 - \frac{1}{2}F\right). \quad (4)$$

Our magnetic samples are expected to be spin-split, whereas the precise level of spin polarization is unknown to us^{28,29}.

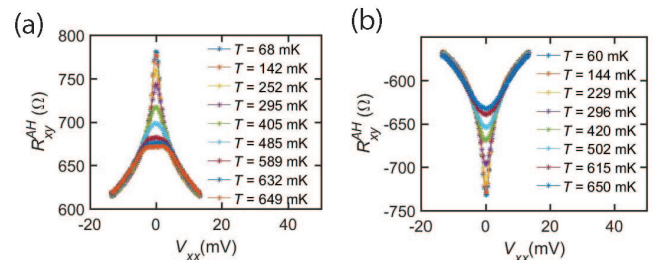


FIG. 4. (color online) Voltage bias dependence of the anomalous Hall effect at several fixed temperatures in V-doped 4 QL thick $(\text{Bi,Sb})_2\text{Te}_3$ films for (a) $B = 7.5\text{T}$ and (b) $B = -7.5\text{T}$.

Fig. 4(a)-(b) further explores the dependence of anomalous Hall effect on both voltage bias and temperature. Increasing either voltage or temperature lowers the anomalous Hall resistance which supports a self-heating mechanism due to applied bias.

We believe that the origin of the non-Ohmic behavior we observe, namely the logarithmic dependence of the conductivity on voltage bias, is fundamentally no different than the logarithmic dependence on temperature and can be understood simply as a consequence of Joule heating. In other words, as the electrons are accelerated by the electric field they inevitably gain energy, and, once they reach a steady state of current flow, this inevitably implies that the electrons possess a larger effective temperature compared to that of the lattice or other reservoirs that serve as heat sinks. By appealing to a simple model of Joule heating³⁹ one can effectively replace the argument of the logarithm in Eq. (1) by $\varepsilon \sim \max(AV^{2/(2+p)}, K_B T, \hbar\omega)$, where V is the voltage bias that drives the transport, A is a constant, and p is the

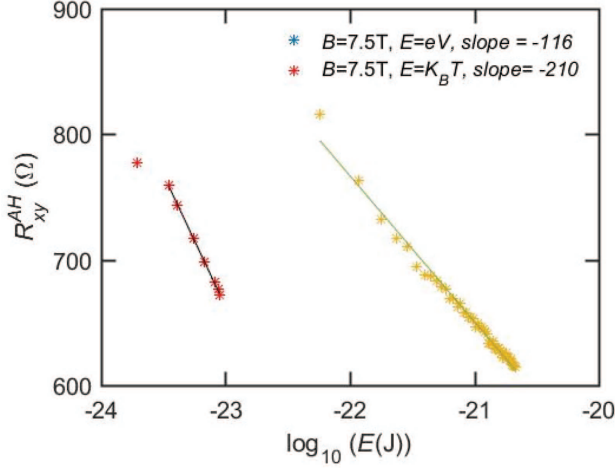


FIG. 5. (color online) Comparison of the dependence of anomalous Hall resistance R_{xy}^{AH} on logarithm of $K_B T$ and eV in V-doped 4 QL thick $(\text{Bi,Sb})_2\text{Te}_3$ films at $B=7.5$ T.

power that controls the temperature dependence of the electron's inelastic scattering rate, $\tau_{in} \propto T^{-p}$. The logarithmic fits of the Hall resistivity vs temperature have approximately twice the slope of those Hall resistivity vs the bias voltage indicating that $p \sim 2$, as shown in Fig. 5.

The Joule heating induced by the bias voltage results to be a more efficient way to tune the electron temperature than the direct control of the temperature of the sample, and, hence we will focus on this dependence for the remainder of the discussion. The expected behavior of the correction to the conductivity for low temperatures dc measurements from the AA theory as a function of voltage is:

$$\delta\sigma_{xx}(V) = \frac{2\kappa}{(2+p)} \frac{e^2}{h} \log(V), \quad \delta\sigma_{xy}(V) = 0. \quad (5)$$

From the data, σ_{xx} and σ_{xy} is calculated using the relations

$$\sigma_{xx} = \frac{\rho_{xx}}{\rho_{xy}^2 + \rho_{xx}^2}, \quad \sigma_{xy} = \frac{\rho_{yx}}{\rho_{xy}^2 + \rho_{xx}^2} \quad (6)$$

where ρ_{xx} and ρ_{xy} are the resistivities considering the square shaped sample geometry. As illustrated in Fig. 6(a), our data is consistent with logarithmic corrections in σ_{xx} while no apparent logarithmic corrections in σ_{xy} , as expected from the AA theory. The anomalous Hall conductivity is nearly quantized at $\pm e^2/h$ as shown in Fig. 6(b). Anecdotally, we argue that quantization of σ_{xy}^{AH} is less sensitive to finite bulk carriers than R_{xy}^{AH} .

To quantify the logarithmic behavior we fit the voltage-dependent nonlinear conductivity as (expressing bias in volts):

$$\sigma_J(V) = \sigma_J^0 + \delta\sigma_J \log(V), \quad J = \{xx, xy\} \quad (7)$$

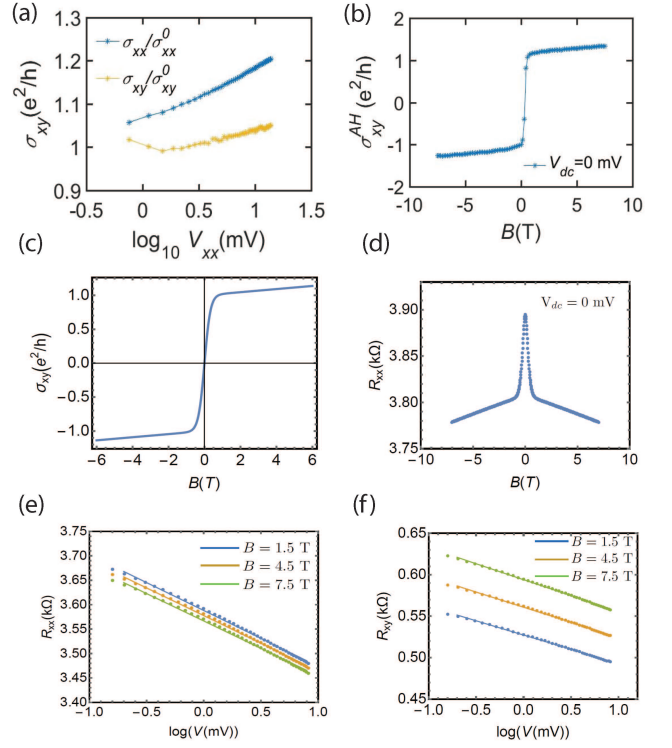


FIG. 6. (color online) Transport coefficients in the V-doped Hall bar (device H_1) as a function of bias. (a) Logarithmic plot for σ_{xx} (blue) and σ_{xy} (orange) at $B=1$ T. (b) Magnetic field dependence of σ_{xy} at $V_{dc}=0$. (c), (d) Theoretical model of the magnetic field dependence of σ_{xy} and R_{xx} . (e), (f) Simulation of dependence of R_{xx} and R_{xy} on bias at $B=1.5$ T, 4.5 T and 7.5 T as expected from interaction corrections in disordered 2D films.

we obtain $\sigma_{xx}^0 \approx 9.17e^2/h$, $\delta\sigma_{xx} \approx 0.33e^2/h$, and $\sigma_{xy}^0 \approx 1.58e^2/h$, $\delta\sigma_{xy} \approx 0.02e^2/h$. Notice the smallness of the bias dependence of σ_{xy} compared to σ_{xx} . Therefore, considering that it is possible that small systematic errors can arise from mixing of R_{xx} and R_{xy} (e.g. if contacts are slightly misaligned R_{xy} picks a small contribution from R_{xx}), we conclude that our data is consistent with σ_{xy} having negligible logarithmic bias dependence and while having significant logarithmic bias dependence on σ_{xx} , as expected from the AA theory. We observe, however, an interesting quantitative deviation from the expectation of the AA theory. Using the approximate value of $p \sim 2$, obtained by comparing the temperature and the voltage fits (see Fig. 5), the fitted parameter κ reads as:

$$\pi\kappa_{\text{fit}} \sim 2. \quad (8)$$

However, from Eqs.(2)-(4), we expect $\pi\kappa \leq 1$, under the natural assumption of repulsive interactions $F > 0$. The origin of this discrepancy is at present unknown to us, but we wish to remind the reader that the equations of the AA we have employed were derived for parabolic electrons without Berry phase effects, and, it remains to be

determined whether nontrivial orbital coherence, such as those giving rise to Berry curvatures for the bands of interest here, affect in any way the classic results of the AA theory.

A simple modeling of the resistivity can be done by using the expected conductivity behavior from the AA theory. The resistivity is taken to be of the form: $\sigma_{xx} = \sigma_{xx}^0 + \delta\sigma_{xx}^0 \log(|V| + V_0)$, where $V_0 \sim 0.4$ mV is essentially a cutoff of the logarithm at small bias (which is controlled by the temperature scale T_0 and the constant A in the Joule heating model), and σ_{xx}^0 and $\delta\sigma_{xx}^0$ are field and bias independent quantities obtained by linear fitting of the logarithmic plots of the conductivity⁴⁰. We add a simple description of the anomalous hall effect in which the Hall conductivity has a jump of e^2/h near zero applied magnetic field in addition to the usual linear term reflecting the classical Hall effect. σ_{xy} in the model is presented in Fig. 6(c) and has the form: $\sigma_{xy} = \frac{e^2}{h} \tanh(B/B_0) + \delta\sigma_{xy}^0 B$, where $B_0 \sim 0.3$ T reflects broadening of the jump of the magnetization as a function of field and $\delta\sigma_{xy}^0$ is field and bias independent. The model is able to reproduce the essential behavior of the resistivities and it is shown in Fig. 6(d) - Fig. 6(f).

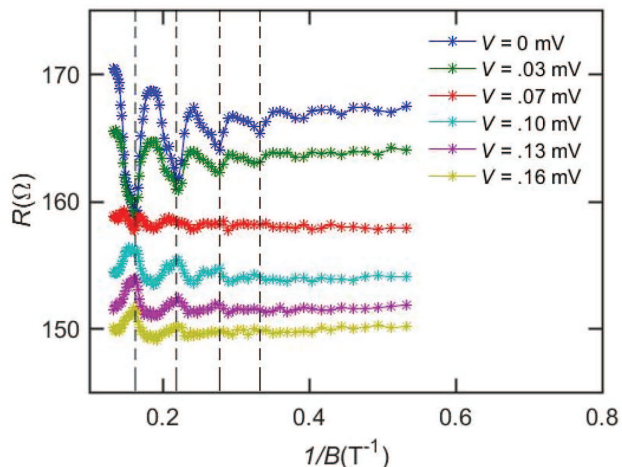


FIG. 7. (color online) Voltage bias dependence of quantum oscillations from magnetoresistance in V-doped $(\text{Bi,Sb})_2\text{Te}_3$ device D_1 of width $W=0.2 \mu\text{m}$.

The transport results discussed above are for larger Hall bar ($\sim 20 \mu\text{m}$) samples. Interestingly, when the device dimension was reduced to submicron range, prominent Shubnikov-de Haas (SdH) oscillations were observed. For example, in a $0.2 \mu\text{m}$ wide device (device D_1) measured by two terminal the oscillations were periodic in $1/B$ and have a non-trivial dependence on bias voltage. These quantum oscillations were seen in multiple samples with Ti/Nb/NbN and Ti/Al contacts. In particular, the zero bias minima turn into maxima in resistance at large voltage bias as shown in Fig. 7.

We also studied the effect of temperature on the magneto-oscillations as shown in Fig. 8. The ampli-

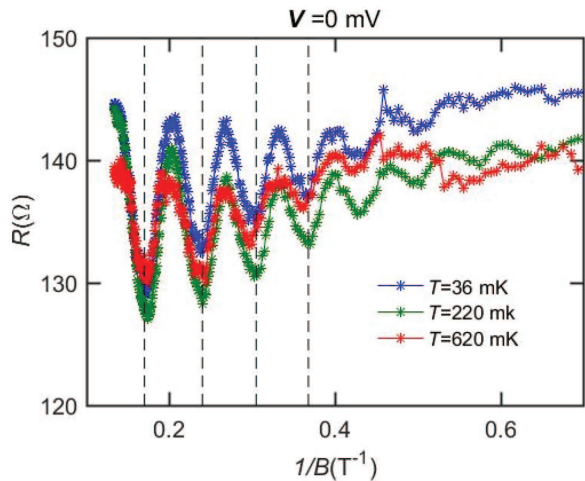


FIG. 8. (color online) Temperature dependence of quantum oscillations from magnetoresistance in V-doped $(\text{Bi,Sb})_2\text{Te}_3$ device D_1 of width $W=0.2 \mu\text{m}$.

tude of the quantum oscillations is found to decrease with increase in temperature. However, the transition from maxima to minima could not be observed at temperatures accessible in the dilution fridge. The inferred electron density is $9 \times 10^{11} \text{ cm}^{-2}$ ($4.5 \times 10^{11} \text{ cm}^{-2}$) for spinful (spinless) Fermions. The period of the SdH could not be changed by applying a backgate or topgate. The screening of the top and bottom gates by the surface states results in inability to change the Fermi energy of the bulk states as has been observed in other topological materials⁴¹. An estimate of the electron gas mobility is made from the onset magnetic field of the SdH oscillations $\mu_q \approx \frac{1}{B_q} \approx 6,000 \text{ cm}^2 \text{ V}^{-1}\text{s}^{-1}$ for the 200 nm wide device⁴². This mobility is intriguingly large compared to macroscopic samples.

We describe a transport model for the non-trivial dependence of the quantum oscillations on voltage bias that we have observed in the narrow junctions. We assume the magneto-conductance to be given by

$$g(B, V) = g_0 + \alpha \rho(\epsilon_F, B) \ln(\epsilon\tau/\hbar) \quad (9)$$

where g_0 is assumed to be a constant background conduction and $\rho(\epsilon_F, B)$ is the SdH density of states given by

$$\rho(\epsilon_F, B) = \frac{2eB}{h} \sum_{j=0}^{j=\infty} \frac{1}{(2\pi)^{1/2}\Gamma} \exp\left(-\frac{(\epsilon_F - \epsilon_j)^2}{2\Gamma^2}\right) \quad (10)$$

where Γ is the half-width of Landau level broadening and ϵ_j is the single particle Landau level energy⁴³. Presence of both bulk and surface conduction mechanisms in topological insulators has been found previously⁴⁴⁻⁴⁹. Fig. 9(a) and Fig. 9(b) display the magneto-transport data normalized to zero bias and zero magnetic field. Similarly, in the model, the resistance $r(B, V) = 1/g(B, V)$ is normalized to its value at zero bias voltage and magnetic field as is shown in Fig. 9(c) and Fig. 9(d) respectively.

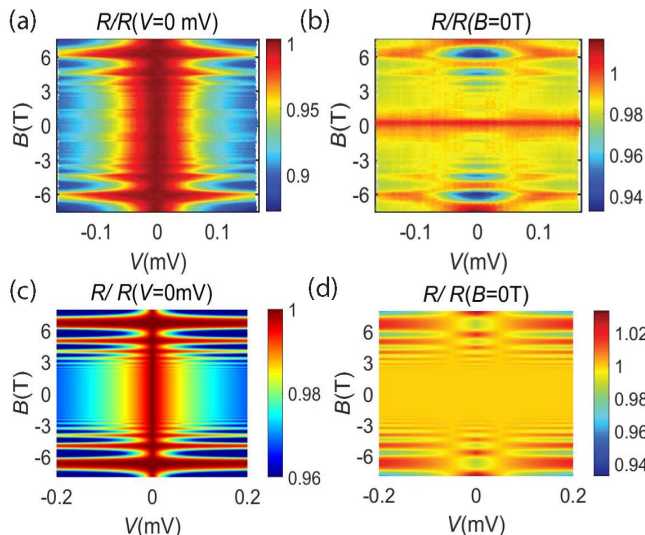


FIG. 9. (color online) (a),(b) The resistance in V-doped $(\text{Bi,Sb})_2\text{Te}_3$ device D_1 is normalized to its zero bias value and normalized to its zero magnetic field value respectively. The evolution is studied with magnetic field and applied bias voltage. The SdH oscillations are present both at small and large bias voltages. However, the zero bias maxima become minima at large bias voltages at a fixed magnetic field and vice versa. (c) A model with two conduction mechanisms in parallel that incorporates logarithmic decay with applied bias of the SdH oscillations on top of a constant background conduction. The resistance is normalized to the zero bias value for comparison to the experimental data. (d) The two conduction model captures the evolution from maxima to minima of the resistance normalized to the zero magnetic field value with voltage bias.

While we do have an understanding of the voltage dependence of the oscillations, there are properties that are less well understood. The contrast of the quantum oscillations is found to decrease systematically with increasing width. Such dependence of visibility of quantum oscillations on channel width is unusual. The quantum oscillations are discussed in further detail in supplementary materials⁴⁰.

IV. CONCLUSION

We have studied magnetotransport in V-doped $(\text{Bi,Sb})_2\text{Te}_3$ and find logarithmic singularities in longitudinal resistance R_{xx} and anomalous Hall resistance R_{xy}^{AH} which is well explained quantitatively by quantum corrections due to electron-electron interactions. In sub-micron scale devices, SdH oscillations are observed where the maxima transition to minima with voltage bias. A simple transport model explains these observations.

V. ACKNOWLEDGEMENTS

The authors acknowledge insightful discussions with Ashwin Viswanathan, Liang Fu, Brian Skinner, Toeno Vander Saar, Lucas Orona and Anindya Das. The authors are grateful to Di S. Wei, Tony X. Zhou, Pat Gunman and Andrei Levin for invaluable help with developing the sample fabrication. AY, DN, KS and JW acknowledge the support from Gordon and Betty Moore Foundation Grant No. 4531, ARO Grant No. W 911 NF-16-1-0491, DOE Grant No. DE-SC0001819 and ARO Grant No. W911NF-17-1-0023. AY also acknowledges support in part by the U. S. Army Research Laboratory and the U. S. Army Research Office under Grant No. W911NF-16-1-0491. IS acknowledges support from MIT Pappalardo Fellowship. PK, GH and KH acknowledge support from NSF Grant No. DMR-1420634. JSM, CZC and YO acknowledge the support from NSF Grant No. DMR-1700137, ONR Grant No. N00014-16-1-2657.

VI. SUPPLEMENTAL MATERIALS FOR 'LOGARITHMIC SINGULARITIES AND QUANTUM OSCILLATIONS IN MAGNETICALLY DOPED TOPOLOGICAL INSULATORS'

A. Processing of $(\text{Bi,Sb})_2\text{Te}_3$ on SrTiO_3 substrate

We developed ebeam fabricated devices of pristine and magnetic topological insulators. This included several challenges including SrTiO_3 being highly insulating, $(\text{Bi,Sb})_2\text{Te}_3$ degrading at elevated temperatures and oxidation of the sample without proper capping layer. Here we report the details of sample processing which would allow several design exploration in the field of topological insulators. The device processing illustrated in Fig. 10 compares favourably to scratched Hall bar devices and does not effect the film quality.

1. Recipe for etching

To etch 4 quintuple layers of pristine and V-doped $(\text{Bi,Sb})_2\text{Te}_3$ with 10 nm Te capping layer, an etch mask of photoresist S1813 is used. Using a laser writer, the mask pattern is defined followed by development in developer CD-26. A 5 mins O_2 plasma etch removes the topological insulator film exposing the transparent SrTiO_3 .

2. Making electrical contact

SrTiO_3 is insulating because of which charging effects are a major concern for high resolution lithography. For patterning the contacts by ebeam lithography, the resist layers of PMMA C6 495 K and PMMA A4 950 K are baked at 100°C as higher temperatures lead to sample

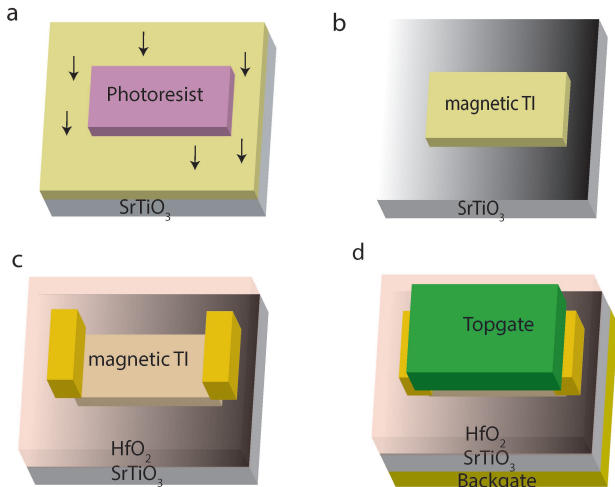


FIG. 10. Schematic of the ebeam fabrication process of topological insulators. (a) The etch mask is patterned photolithographically from photoresist S1813 by UV exposure. (b) The unprotected topological insulator film is removed by oxygen plasma. (c) Superconducting or normal metal contacts are ebeam lithographically patterned and metallized. Subsequently, a high κ dielectric of HfO_2 is grown by atomic layer deposition. (d) A topgate as well as a backgate of Ti/Au is deposited.

degradation. Then 10 nm of Al is deposited for reducing charging effects which is transparent under scanning electron microscope imaging. After ebeam exposure, the Al is removed in AZ 400K developer in 5 mins and then developed in MIBK : IPA (1 : 3). As the topological insulator film is protected from oxidation by an insulating capping layer, an in-situ argon plasma etch is done before deposition of Ti(10 nm)/Au(100 nm) or Ti (10 nm)/Nb(5 nm)/NbN(50 nm). Optimization of the etch time is necessary to make good electrical contact to the film.

3. Making topgated devices

After electrical contacts are made, a 20 nm HfO_2 dielectric is grown by atomic layer deposition (ALD) at 80 ° C. A Ti (10 nm)/Au(100 nm) topgate is deposited on top of the HfO_2 dielectric. The topgated devices can be effectively tuned through the charge neutrality point.

4. Making backgates

After the topside fabrication is complete, the device is coated with PMMA C6 495 K baked at 100 ° C and flipped over to deposit Ti(10 nm)/Au(100 nm) backgate. The protecting ebeam resist is then dissolved and the device is wirebonded.

B. Measuring the contact resistance by transfer length method

The two terminal resistance to the pristine and magnetic topological insulator film is measured as a function of various gap sizes W . By extrapolating to gap size $W = 0$, the residual resistance is measured. The equation used to determine the contact resistances by transfer length method are^{50,51}:

$$R_{total} = \rho_{sheet} \frac{W}{d} + 2R_c \quad (11)$$

where ρ_{sheet} is the sheet resistance. In this technique, we conclude that the contact resistance is below 50 Ω at 4.2 K and makes good electrical contact to the film.

C. Topgating of magneto-oscillations

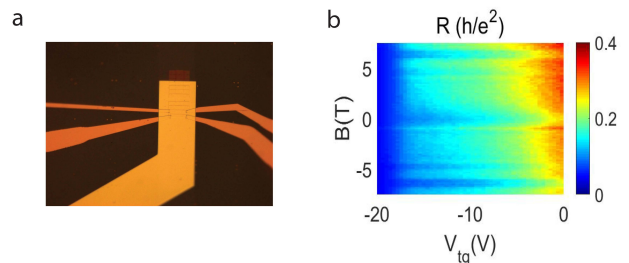


FIG. 11. (a) Optical microscope image of topgated topological insulator film with 20 nm HfO_2 dielectric. (b) Two terminal resistance in Ti/Nb/NbN devices show significant topgate response. Intriguingly, the magneto-oscillations in B -field do not depend on changes in topgate voltages.

We integrate ALD grown high- k dielectric on pristine and magnetic topological insulators which allows to tune the Fermi-energy. The ALD deposition of 20 nm HfO_2 dielectric is done at 80° C to avoid any sample degradation due to overheating. All topgated devices could be tuned through charge neutrality. Intriguingly, the magnetic field dependence of the quantum oscillations was independent of the topgate voltage as shown in Fig. 11.

D. Estimating density and mean free path

Fig. 12 shows the Hall resistance R_{xy} for Hall-bar sample (taken near zero bias) as a function of magnetic field. By making a linear fit to the large field values (shown as a dashed line) we can estimate the sample density using the semiclassical value of the Hall resistivity: $R_{xy} = B/nec$. From this we infer a carrier density of $n \approx 8.3 \times 10^{17} \text{m}^{-2}$. To estimate the elastic mean free path we use the values of the longitudinal resistance R_{xx} for the Hall-bar sample (taken near zero bias) as depicted in Fig. 13. using the formula:

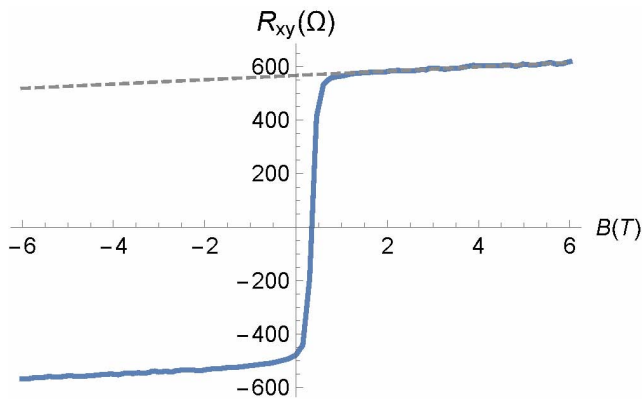


FIG. 12. (color online) R_{xy} for Hall-bar sample as a function of magnetic field.

$$k_F l = \frac{2R_K}{g\rho_{xx}}, \quad (12)$$

where R_K the Von-Klitzing's constant $R_K = 25k\Omega$ and $g = \{1, 2\}$ for spinless/spinfull electrons. Assuming the sample to be squared (we only want a rough order of magnitude for the mean free path), and taking $R_{xx} \sim 4.3k\Omega$, we obtain $k_F l \sim \{12, 6\}$ for spinless/spinfull electrons. So, we expect an elastic mean free path of about $l \sim \{3.7nm, 2.6nm\}$. This estimate implies that the sample is rather clean, and perturbative calculations on $1/(k_F l)$ are expected to capture the essential transport behavior.

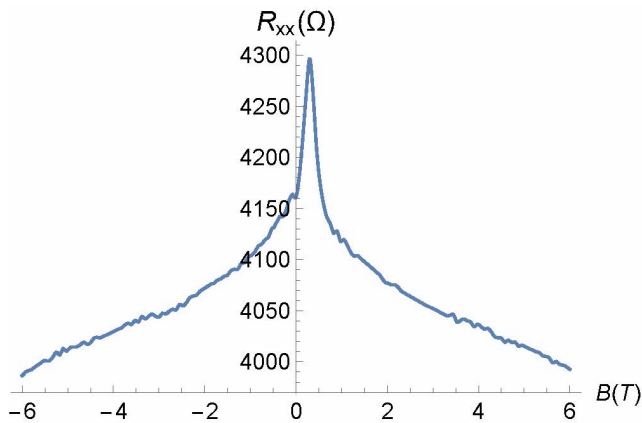


FIG. 13. (color online) R_{xx} for Hall-bar sample as a function of magnetic field.

To quantify this more precisely we estimate the localization length, which for a 2D system can be estimated as⁵²:

$$\xi \sim l \exp\left(\frac{1}{2}\pi k_F l\right) \quad (13)$$

and is about $\xi \sim \{3.2 \times 10^{-5}m, 0.6m\}$ for our Hall bar samples. This length scale needs to be compared with a

density diffusion length relevant for the Altshuler-Aronov theory of interaction corrections, which, near zero bias, can be taken to be controlled by the temperature of the sample and is given by²⁹:

$$L_\epsilon \sim \sqrt{\frac{\hbar D}{k_B T}} \sim \sqrt{\frac{\hbar v_F l}{2k_B T}}, \quad D = \frac{\tau v_F^2}{2} = \frac{lv_F}{2} \quad (14)$$

For a typical sample temperature of $T \sim 50mK$ and using the fermi velocity of a TI with 4 QL's⁵³ ($v_F \sim 4.5 \times 10^5 m/s$), we obtain an interaction length: $L_\epsilon \sim \{3 \times 10^{-7}m, 3.6 \times 10^{-7}m\}$. Therefore the dimensionless parameter $\log(L_\epsilon/l)/\log(\xi/l) \sim \{0.5, 0.2\}$ is found to be reasonably small lending confidence to the applicability^{29,52} of the Altshuler-Aronov theory to our samples. Apart from the difference in localization lengths, the order of magnitude of the estimates of transport coefficients are not very sensitive on whether we assume spinless or spin-full electrons.

E. Electronic structure and range of densities for spinless vs spinful picture

A simple model for the electronic dispersion of the two dimensional electron system arising in thin 2D Ti slabs starts for two flavors of Dirac fermions describing the states in top and bottom surfaces coupled via tunneling. This model is supplemented by a ferromagnetic exchange splitting, and is capable of predicting the quantum anomalous Hall state arising in these systems⁵⁴. The Hamiltonian can be written as:

$$H = \begin{pmatrix} \frac{U}{2} + M_0 & iv(k_x - ik_y) & t & 0 \\ -iv(k_x + ik_y) & \frac{U}{2} - M_0 & 0 & t \\ t & 0 & -\frac{U}{2} + M_0 & -iv(k_x - ik_y) \\ 0 & t & iv(k_x + ik_y) & -\frac{U}{2} - M_0 \end{pmatrix},$$

where M_0 is the exchange splitting induced energy scale, t is the tunneling strength between top and bottom surfaces, U is a possible bias between top and bottom layers developed when an electric field is present across the TI slab, and v is the typical Dirac velocity of the surface states of the TI. There are four bands associated with this Hamiltonian:

$$E_k = \pm \sqrt{v^2 k^2 + M_0^2 + t^2 + (U/2)^2} \pm \sqrt{v^2 k^2 U^2 + M_0^2 (4t^2 + U^2)}. \quad (15)$$

Assuming the field across the slab is negligible ($U \approx 0$), then the dispersion reduces to:

$$E_k = \pm \sqrt{v^2 k^2 + (|M_0| \pm |t|)^2}. \quad (16)$$

The condition for the stability of the topologically non-trivial AQH insulator is: $|M_0| > |t|$ (the state with $|M_0| < |t|$ has a

Chern number 0 and is a trivial insulator). When the system is doped and becomes metallic, the condition the chemical potential must satisfy in order to guarantee that a single band is occupied is $|M_0| + |t| > \mu > |M_0| - |t|$. This condition translates in terms of densities into:

$$|n| < \frac{|M_0||t|}{\pi v^2 \hbar^2}, \quad (17)$$

In other words, for densities within this range a single band is occupied and otherwise two bands are occupied. An estimate for $t \approx 0.06eV$ for a slab of $4QL$ and $v = 4.5 \times 10^5 m/s$ ⁵³. The density (using only t) $\frac{|t|^2}{\pi v^2 \hbar^2} \approx 3.3 \times 10^{10} cm^{-2}$.

- ¹ R. Yu, W. Zhang, H. J. Zhang, S. C. Zhang, X. Dai, and Z. Fang, *Science* **329**, 61 (2010).
- ² C. Z. Chang, J. Zhang, X. Feng, J. Shen, Z. Zhang, M. Guo, K. Li, Y. Ou, P. Wei, L. L. Wang, and et al., *Science* **340**, 167 (2013).
- ³ C. Z. Chang, W. Zhao, D. Y. Kim, H. Zhang, B. A. Assaf, D. Heiman, S. C. Zhang, C. Liu, M. H. W. Chan, and J. S. Moodera, *Nature Materials* **14**, 473 (2015).
- ⁴ M. Mogi, R. Yoshimi, A. Tsukazaki, K. Yasuda, Y. Kozuka, K. S. Takahashi, M. Kawasaki, and Y. Tokura, *Applied Physics Letters* **107**, 182401 (2015).
- ⁵ C. Z. Chang, W. Zhao, D. Y. Kim, P. Wei, J. K. Jain, C. Liu, M. H. W. Chan, and J. S. Moodera, *Phys. Rev. Lett.* **115**, 057206 (2015).
- ⁶ W. K. Tse and A. H. MacDonald, *Phys. Rev. Lett.* **105**, 057401 (2010).
- ⁷ I. Garate and M. Franz, *Phys. Rev. Lett.* **104**, 146802 (2010).
- ⁸ X. L. Qi, R. Li, J. Zang, and S. C. Zhang, *Science* **323**, 1184 (2009).
- ⁹ X. L. Qi, T. L. Hughes, and S. C. Zhang, *Phys. Rev. B* **82**, 184516 (2010).
- ¹⁰ Q. L. He, L. Pan, A. L. Stern, E. C. Burks, X. Che, G. Yin, J. Wang, B. Lian, Q. Zhou, E. S. Choi, *et al.*, *Science* **357**, 294 (2017).
- ¹¹ Y. L. Chen, J. H. Chu, J. G. Analytis, Z. K. Liu, K. Igarashi, H. H. Kuo, X. L. Qi, S. K. Mo, R. G. Moore, D. H. Lu, *et al.*, *Science* **329**, 659 (2010).
- ¹² S. Y. Xu, M. Neupane, C. Liu, D. Zhang, A. Richardella, L. A. Wray, N. Alidoust, M. Leandersson, T. Balasubramanian, J. Sánchez Barriga, *et al.*, *Nature Physics* **8**, 616 (2012).
- ¹³ Z. Jiang, C. Z. Chang, C. Tang, P. Wei, J. S. Moodera, and J. Shi, *Nano letters* **15**, 5835 (2015).
- ¹⁴ F. Katmis, V. Lauter, F. S. Nogueira, B. A. Assaf, M. E. Jamer, P. Wei, B. Satpati, J. W. Freeland, I. Eremin, D. Heiman, *et al.*, *Nature* **533**, 513 (2016).
- ¹⁵ C. Tang, C. Z. Chang, G. Zhao, Y. Liu, Z. Jiang, C. X. Liu, M. R. McCartney, D. J. Smith, T. Chen, J. S. Moodera, *et al.*, *Science Advances* **3**, e1700307 (2017).
- ¹⁶ Y. S. Hor, P. Roushan, H. Beidenkopf, J. Seo, D. Qu, J. G. Checkelsky, L. A. Wray, D. Hsieh, Y. Xia, S. Y. Xu, D. Qian, M. Z. Hasan, N. P. Ong, A. Yazdani, and R. J. Cava, *Phys. Rev. B* **81**, 195203 (2010).
- ¹⁷ J. K. Viljas and T. T. Heikkilä, *Phys. Rev. B* **81**, 245404 (2010).
- ¹⁸ M. Liu, W. Wang, A. R. Richardella, A. Kandala, J. Li, A. Yazdani, N. Samarth, and N. P. Ong, *Science advances* **2**, e1600167 (2016).
- ¹⁹ N. Samarth, *Nature Materials* **16**, 1068 (2017).
- ²⁰ J. Chen, H. J. Qin, F. Yang, J. Liu, T. Guan, F. M. Qu, G. H. Zhang, J. R. Shi, X. C. Xie, C. L. Yang, K. H. Wu, Y. Q. Li, and L. Lu, *Phys. Rev. Lett.* **105**, 176602 (2010).
- ²¹ S. P. Chiu and J. J. Lin, *Phys. Rev. B* **87**, 035122 (2013).
- ²² S. Hikami, A. I. Larkin, and Y. Nagaoka, *Progress of Theoretical Physics* **63**, 707 (1980).
- ²³ H. T. He, G. Wang, T. Zhang, I. K. Sou, G. K. L. Wong, J. N. Wang, H. Z. Lu, S. Q. Shen, and F. C. Zhang, *Phys. Rev. Lett.* **106**, 166805 (2011).
- ²⁴ M. Liu, J. Zhang, C. Z. Chang, Z. Zhang, X. Feng, K. Li, K. He, L. L. Wang, X. Chen, X. Dai, Z. Fang, Q. K. Xue, X. Ma, and Y. Wang, *Phys. Rev. Lett.* **108**, 036805 (2012).
- ²⁵ H. Z. Lu, J. Shi, and S. Q. Shen, *Phys. Rev. Lett.* **107**, 076801 (2011).
- ²⁶ G. Bergmann, *Physics Reports* **107**, 1 (1984).
- ²⁷ B. L. Altshuler, D. E. Khmel'nitzkii, A. I. Larkin, and P. A. Lee, *Phys. Rev. B* **22**, 5142 (1980).
- ²⁸ P. A. Lee and T. V. Ramakrishnan, *Rev. Mod. Phys.* **57**, 287 (1985).
- ²⁹ B. L. Altshuler and A. G. Aronov, *Electron-electron interactions in disordered systems* (edited by A. L. Efros and M. Pollak (North-Holland, Amsterdam, 1985)).
- ³⁰ H. Fukuyama, *Journal of the Physical Society of Japan* **49**, 644 (1980).
- ³¹ P. W. Anderson, *Physical Review* **124**, 41 (1961).
- ³² J. Kondo, *Progress of theoretical physics* **32**, 37 (1964).
- ³³ J. Appelbaum, *Physical Review Letters* **17**, 91 (1966).
- ³⁴ M. Liu, C. Z. Chang, Z. Zhang, Y. Zhang, W. Ruan, K. He, L. L. Wang, X. Chen, J. F. Jia, S.-C. Zhang, *et al.*, *Physical review B* **83**, 165440 (2011).
- ³⁵ J. Wang, A. M. DaSilva, C. Z. Chang, K. He, J. K. Jain, N. Samarth, X. C. Ma, Q. K. Xue, and M. H. W. Chan, *Physical Review B* **83**, 245438 (2011).
- ³⁶ B. L. Altshuler and A. G. Aronov, *Solid State Communications* **30**, 115 (1979).
- ³⁷ B. L. Altshuler, A. G. Aronov, and D. E. Khmel'nitsky, *Journal of Physics C: Solid State Physics* **15**, 7367 (1982).
- ³⁸ B. L. Altshuler, A. G. Aronov, and P. A. Lee, *Phys. Rev. Lett.* **44**, 1288 (1980).
- ³⁹ E. Abrahams, P. W. Anderson, and T. V. Ramakrishnan, *Philosophical Magazine B* **42**, 827 (1980).
- ⁴⁰ See Supplementary Materials at.
- ⁴¹ D. M. Mahler, J. Wiedenmann, C. Thienel, F. Schmitt, C. Ames, R. Schlereth, P. Leubner, C. Brune, H. Buhmann, D. D. Sante, C. Gould, G. Sangiovanni, and L. W. Molenkamp, preprint (2017).
- ⁴² X. Cui, G. H. Lee, Y. D. Kim, G. Arefe, P. Y. Huang, C. H. Lee, D. A. Chenet, X. Zhang, L. Wang, F. Ye, *et al.*, *Nature nanotechnology* **10**, 534 (2015).
- ⁴³ J. P. Eisenstein, H. L. Stormer, V. Narayanamurti, A. Y. Cho, A. C. Gossard, and C. W. Tu, *Phys. Rev. Lett.* **55**, 875 (1985).
- ⁴⁴ J. G. Analytis, R. D. McDonald, S. C. Riggs, J. H. Chu, G. S. Boebinger, and I. R. Fisher, *Nature Physics* **6**, 960

- (2010).
- ⁴⁵ J. G. Analytis, J. H. Chu, Y. Chen, F. Corredor, R. D. McDonald, Z. X. Shen, and I. R. Fisher, [Physical Review B](#) **81**, 205407 (2010).
- ⁴⁶ D. X. Qu, Y. S. Hor, J. Xiong, R. J. Cava, and N. P. Ong, [Science](#) **329**, 821 (2010).
- ⁴⁷ J. Xiong, Y. Luo, Y. H. Khoo, S. Jia, R. J. Cava, and N. P. Ong, [Physical Review B](#) **86**, 045314 (2012).
- ⁴⁸ H. Cao, J. Tian, I. Miotkowski, T. Shen, J. Hu, S. Qiao, and Y. P. Chen, [Physical review letters](#) **108**, 216803 (2012).
- ⁴⁹ K. Saha and I. Garate, [Phys. Rev. B](#) **90**, 245418 (2014).
- ⁵⁰ A. Venugopal, L. Colombo, and E. M. Vogel, [Applied Physics Letters](#) **96**, 013512 (2010).
- ⁵¹ L. Wang, I. Meric, P. Y. Huang, Q. Gao, Y. Gao, H. Tran, T. Taniguchi, K. Watanabe, L. M. Campos, D. A. Muller, *et al.*, [Science](#) **342**, 614 (2013).
- ⁵² P. A. Lee and T. V. Ramakrishnan, [Rev. Mod. Phys.](#) **57**, 287 (1985).
- ⁵³ Y. Zhang, K. He, C. Z. Chang, C. L. Song, L. L. Wang, X. Chen, J. F. Jia, Z. Fang, X. Dai, W. Y. Shan, *et al.*, [Nature Physics](#) **6**, 584 (2010).
- ⁵⁴ R. Yu, W. Zhang, H. J. Zhang, S. C. Zhang, X. Dai, and Z. Fang, [Science](#) **329**, 61 (2010).